ECS Transactions, 35(3) 185-192 (2011)
10.1149/1.3569910 © The Electrochemical Society

An Investigation of the Geometrical Effects on the Thermal Conductivity of Graphene Antidot Lattices

H. Karamitaheri[a], M. Pourfath[b], R. Faez[a], and H. Kosina[b]

[a] School of Electrical Engineering, Sharif University of Technology, Tehran, Iran
[b] Institute for Microelectronics, TU Wien, Wien, Austria

In this work we investigate the thermal conductivity of graphene-based antidot lattices. A third nearest-neighbor tight-binding model and a forth nearest-neighbor force constant model are employed to study the electronic and phononic band structures of graphene-based antidot lattices. Ballistic transport models are used to evaluate the electronic and the thermal conductivities. Methods to reduce the thermal conductivity and to increase the thermoelectric figure of merit of such structures are studied. Our results indicate that triangular antidot lattices have the smallest thermal conductivity due to longer boundaries and the smallest distance between the neighboring dots.

Introduction

Progress in nanomaterials synthesis has allowed the realization of low-dimensional thermoelectric device structures such as one-dimensional nanowires, thin films, and two-dimensional superlattices (1–4). The efficiency of thermoelectric devices for converting waste heat into useful electrical energy depends on the figure of merit ZT. This figure is defined as $ZT = S^2\sigma T/(K_{\mathrm{el}} + K_{\mathrm{ph}})$, with the Seebeck coefficients S, the electrical conductivity σ, temperature T, and the electrical and lattice contributions to the thermal conductivity K_{el} and K_{ph}, respectively (5). The numerator of Z is called power factor. The figure of merit determines the efficiency of a thermoelectric device and can be improved by increasing the power factor and decreasing the thermal conductivity.

Bismuth and its alloys have been studied and used as thermoelectric materials for many years (6) due to their low thermal conductivity. Nevertheless, the use of heavy metals in large scale applications is limited. On the contrary, bulk Silicon that benefits from the availability of large scale manufacturing processes, has a very low $ZT \approx 0.01$ (7). Large improvements in ZT have been reported in Silicon nanowires ($ZT \approx 1$) (1, 2, 8). In addition, very recent studies show that by introducing holes into bulk Silicon the thermal conductivity can be strongly suppressed and ZT can be enhanced by two orders of magnitude (9).

Many studies have been conducted to investigate mechanisms that affect the thermal conductivity, such as the effects of boundaries (10), isotope doping (11, 12), defects (13) and the Hydrogen termination (10). These studies indicate that the thermal conductivity can be significantly reduced by the creation of defects and isotope doping, specially in the low doping regime (11). The role of boundaries and edge states has been studied (14, 15). The results indicate that in the presence of edge disorder the thermoelectric figure of merit can significantly increase.

Graphene, a recently discovered form of carbon that consists of only one layer of atoms arranged in a honeycomb lattice (16), has received much attention in the last few years for its interesting electrical (17, 18), optical (18–20), and thermal (21–23) properties. Recently a large scale method to produce graphene sheets has been reported (24). The electrical conductivity of a graphene sheet is as high as that of copper (25). A giant Seebeck coefficient has been reported for graphene (26). These factors render graphene as a candidate for future energy harvesting applications. However, the ability of graphene to conduct heat is an order of magnitude higher than that of copper (21). Therefore, it is necessary to reduce its thermal conductivity. The high thermal conductivity of graphene is mostly due to the lattice contribution, whereas the electronic contribution to the thermal conduction can be ignored (21, 27, 28). Therefore, by proper engineering of phonon transport it is possible to reduce the total thermal conductivity without significant reduction of the electrical conductivity and the power factor. In this work we investigate the thermal conductivity of graphene-based antidot lattices (29) (GALs). We show that by introducing dots in the graphene sheet (Fig. 1) the thermal conductivities of GALs decrease and the respective ZT values increase.

Graphene Antidot Lattices

The electrical and optical properties of GALs have been theoretically studied in Refs. (19, 30, 31). The results indicate that by introducing regular dots in a graphene sheet, it is possible to achieve a direct band gap semiconductor from a semi-metal pristine graphene sheet. Bai and co-workers reported the first field-effect-transistor based on GALs (29). In this paper we investigate the effect of the dot geometry on the thermal conductivity of GALs. The unit cell of a GAL can be described by two parameters L and N, where L is the side length of the hexagon in terms of the graphene lattice constant $a = 2.46\mathring{A}$, and N is the number of carbon atoms that are removed from the pristine supercell. In Fig. 1 Circ, Rect, Hex, IsoTri, and RightTri indicate a circular, rectangular, hexagonal, iso-triangular, and right-triangular dot in the hexagonal unit cell, respectively. Fig. 1-b shows a circular antidot which is formed by removing 108 carbon atoms from a cell with $L = 10$. Therefore, it is represented by Circ$(10, 108)$. For a fair comparison, we keep the area of different dots within 15%. Therefore, the number of carbon atoms that are removed from the pristine unit cell is nearly equal for different unit cells.

The Electronic and Phononic Band Structure

To describe the electronic band structure of GALs, a three nearest-neighbor tight-binding approximation is employed (32). The hopping parameter for the first and third nearest-neighbor are assumed to be -3.2eV and -0.3eV, respectively, and for the second nearest-neighbor a zero hopping parameter is considered (32).

A dynamical matrix can be used to describe the dispersion relation of phonons:

$$D^{ij}(k) = \left(\sum_l K^{il} - M_i \omega^2(k) I \right) \delta_{ij} - \sum_l K^{il} e^{i\mathbf{k}\cdot\Delta\mathbf{R}_{il}} \qquad [1]$$

where M_i is the atomic mass of the i^{th} carbon atoms, $\Delta\mathbf{R}_{ij} = \mathbf{R}_i - \mathbf{R}_j$ is the relative coordinate of the i^{th} atom with respect to the j^{th} atom, and K^{ij} is a 3×3 force constant

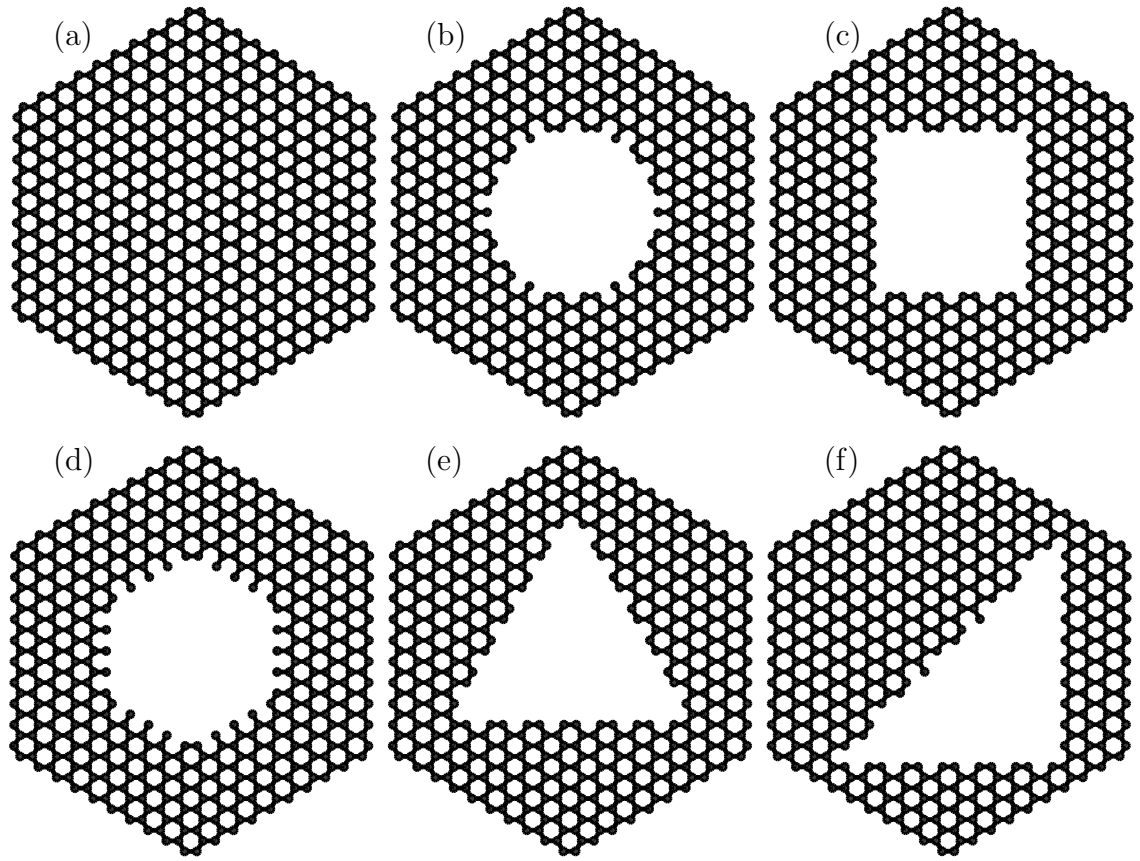

Figure 1: Geometrical structrues of different GALs. (a)-(f) indicate a pristine graphene, Circ(10, 108), Rect(10, 120), Hex(10, 120), IsoTri(10, 126), and RightTri(10, 126), respectively.

tensor describing the coupling between the i^{th} and j^{th} carbon atoms, which are the NN^{th} nearest-neighbor of each other:

$$K^{(ij)} = U_m^{-1} \begin{pmatrix} \Phi_r^{(NN)} & 0 & 0 \\ 0 & \Phi_{ti}^{(NN)} & 0 \\ 0 & 0 & \Phi_{to}^{(NN)} \end{pmatrix} U_m \qquad [2]$$

Φ_r, Φ_{ti} and Φ_{to} are the radial, in-plane transverse, and out-of-plane transverse components of the force constant tensor, respectively, and their values are given in Table I (33). U_m is a unitary matrix defined as:

$$U_m = \begin{pmatrix} \cos\Theta_{ij} & \sin\Theta_{ij} & 0 \\ -\sin\Theta_{ij} & \cos\Theta_{ij} & 0 \\ 0 & 0 & 1 \end{pmatrix} \qquad [3]$$

Here, we assume that the graphene sheet is located in the $x-y$ plane and Θ_{ij} represents the angle between the x-axes and the bond of the i^{th} and j^{th} carbon atoms.

Table I: Elements of the force constant tensor (33). The unit is N/m.

NN	Φ_r	Φ_{ti}	Φ_{to}
1	365.0	245.0	98.2
2	88.0	-32.3	-4.0
3	30.0	-52.5	1.5
4	-19.2	22.9	-5.8

Transport Coefficients

The ballistic transport coefficients for GALs can be evaluated using the Landauer formula (34, 35):

$$G = \frac{2q^2}{h} \int_{-\infty}^{+\infty} \overline{T}_{\rm el}(E) \left(-\frac{\partial f}{\partial E}\right) \, dE \qquad [4]$$

$$T\overline{SG} = -\frac{2q}{h} \int_{-\infty}^{+\infty} \overline{T}_{\rm el}(E) \, (E - E_{\rm F}) \left(-\frac{\partial f}{\partial E}\right) \, dE \qquad [5]$$

$$K_0 = \frac{2}{hT} \int_{-\infty}^{+\infty} \overline{T}_{\rm el}(E) \, (E - E_{\rm F})^2 \left(-\frac{\partial f}{\partial E}\right) \, dE \qquad [6]$$

$$K_{\rm ph} = \frac{1}{h} \int_{0}^{+\infty} \overline{T}_{\rm ph}(\omega) \hbar\omega \left(\frac{\partial n(\omega)}{\partial T}\right) \, d(\hbar\omega) \qquad [7]$$

$\overline{T}_{\rm el}(E)$ and $\overline{T}_{\rm ph}(\omega)$ are the electron and phonon transmission probabilities, respectively. One can find the Seebeck coefficient and the electronic contribution to the thermal conductance using $S = \overline{SG}/G$ and $K_{\rm el} = K_0 - TS^2G$, respectively. In the ballistic limit, $\overline{T}_{\rm el}(E)$ and $\overline{T}_{\rm ph}(\omega)$ can be extracted from the density of modes (34).

Results and Discussion

The phonon density of states (DOS) of different GALs are shown in Fig. 2. The DOS of GALs are quite similar and they are slightly smaller than that of a pristine graphene sheet. This can be explained by the fact that the total number of atoms in the unit cell of GALs is nearly the same.

Although the DOS of the GALs have the same order as that of a pristine graphene sheet, the transmission probabilities can be very different. Fig. 3 shows that the phonon transmissions of Circ(10, 108) and Rect(1, 120) are quite different from that of a pristine graphene. However, Circ(10, 108), Rect(10, 120), and Hex(10, 120) have nearly the same transmission probabilities, whereas IsoTri(10, 126) and Right(10, 126) have similar transmissions but different from the first group, see Fig. 4.

The transmission probabilities of Circ(10, 108), Rect(10, 120) and Hex(10, 120) are similar because they have similar circumference and, therefore, the same number of boundary carbon atoms. Furthermore, the nearest-neighbor dots in these GALs have nearly the

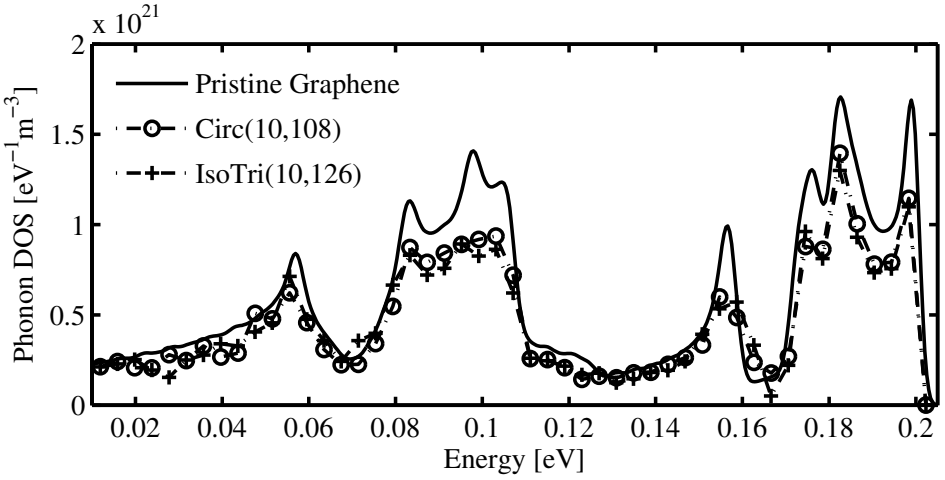

Figure 2: The comparison between the phonon DOS of graphene and GALs. Due to nearly the same of number of atoms in the unit cell of GALs, they have similar DOS.

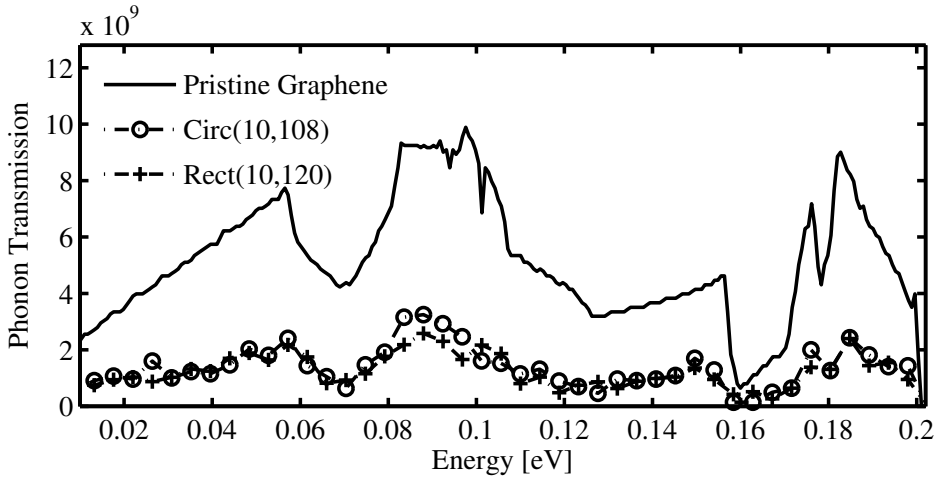

Figure 3: The comparison between the phonon transmission of a pristine graphene, Circ(10, 108), and Rect(10, 120).

same distance. On the other hand, IsoTri(10, 126) and RightTri(10, 126) have the same circumference, but different from the first group. The calculated lattice thermal conductivities of different GALs are presented in Table II. Although the areas of the unit cells of IsoTri(10, 126) and RightTri(10, 126) are nearly the same as that of Hex(10, 120) and Rect(10, 120), their thermal conductivities are 30% smaller. This can be explained by the 25% larger circumference and the smaller distance between nearest dots of IsoTri(10, 126) and RightTri(10, 126).

The figures of merit of different GALs as a function of the Fermi energy are compared in Fig. 5. IsoTri has the highest ZT, because it has the lowest lattice thermal conductivity and largest Seebeck coefficient. At room temperature, the factor $\partial f/\partial E$ is approximately non-zero only in the range of 0.2eV around the Fermi level. Under the condition that

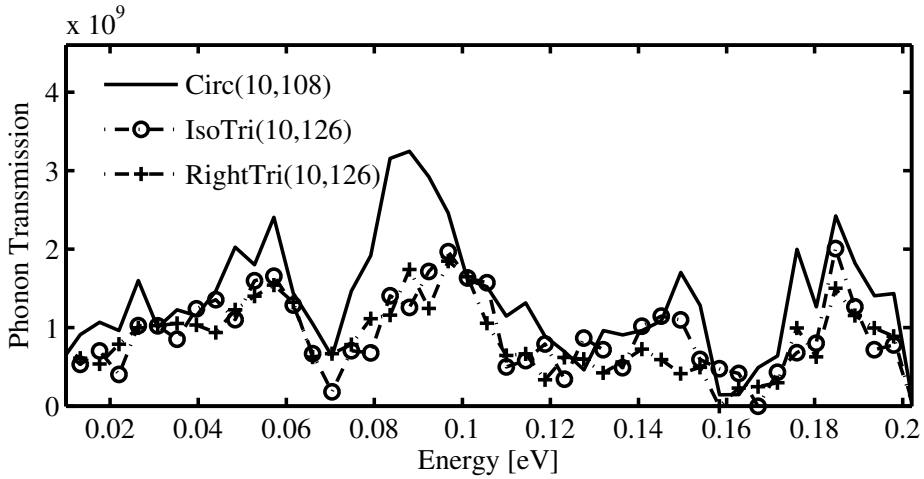

Figure 4: The comparison between the phonon transmission of Circ(10, 108), IsoTri(10, 126), and RightTri(10, 126). IsoTri(10, 126) and RightTri(10, 126) have similar transmission probability, but smaller than that of the Circ(10, 108). This can be explained by a larger circumference and lower distance between the nearest-neighbor dots of these two GALs.

Table II: The comparison of the thermal conductivities of different GALs. The results are normalized to the thermal conductivity of a pristine graphene.

Structure	**Normalized thermal conductance**
Pristine Graphene	1
Circ(10, 108)	0.2694
Rect(10, 120)	0.2462
Hex(10, 120)	0.2696
IsoTri(10, 126)	0.1916
RightTri(10, 126)	0.1834

$E_{\mathrm{G}} > 0.2$eV, holes have no contribution to the total electrical current. A large value of Seebeck coefficient is therefore obtained.

In our work we did not consider the passivation of dangling bonds at the edges. However, it has been shown that Hydrogen passivation of dangling bonds results in the further reduction of the thermal conductivity (10). Therefore, a higher ZT for GALs can be obtained by edge passivation.

Conclusions

Our results indicate that the size of the dots, the circumference of the dots, and the distance between dots can strongly influence the thermal properties of graphene antidot lattices. We show that by appropriate selection of the geometrical parameters one can significantly reduce the thermal conductivity of graphene antidot lattices and improve their thermoelectric figure of merit.

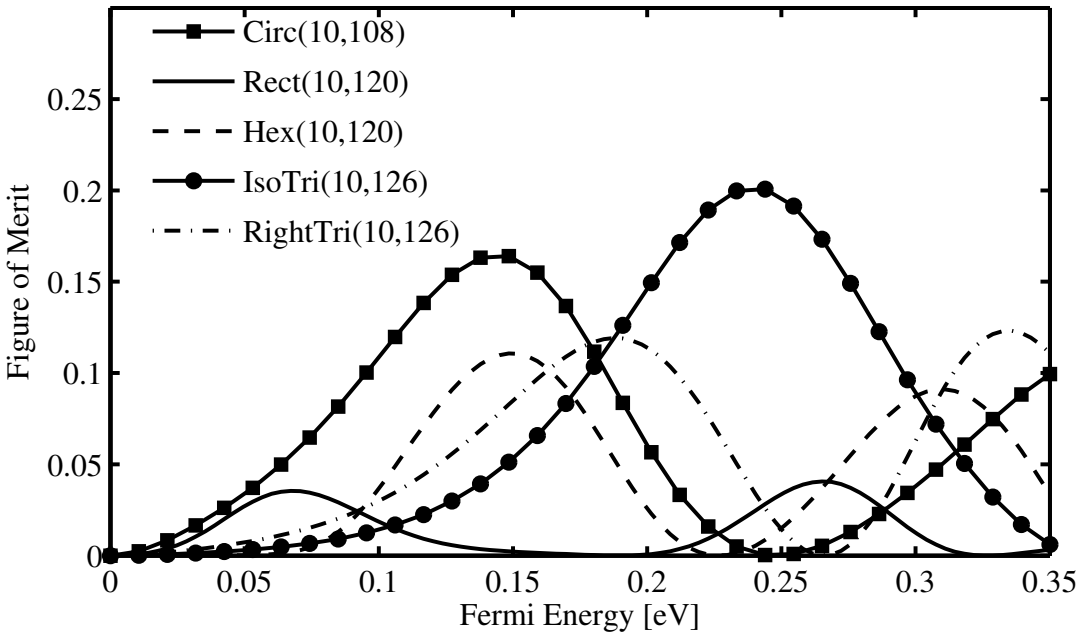

Figure 5: The figure of merit of different GALs as a function of the Fermi energy.

Acknowledgment

This work, as part of the ESF EUROCORES program EuroGRAPHENE, was partly supported by funds from FWF, contract I420-N16.

References

1. A. I. Hochbaum, R. Chen, R. D. Delgado, W. Liang, E. C. Garnett, M. Najarian, A. Majumdar, and P. Yang, *Nature* **451**, 163–168 (2008).
2. A. I. Boukai, Y. Bunimovich, J. T.-Kheli, J.-K. Yu, W. A. G. III, and J. R. Heath, *Nature* **451**, 168–171 (2008).
3. R. Venkatasubramanian, E. Siivola, T. Colpitts, and B. O'Quinn, *Nature* **413**, 597–602 (2001).
4. W. Kim, S. L. Singer, A. Majumdar, D. Vashaee, Z. Bian, A. Shakouri, G. Zeng, J. E. Bowers, J. M. O. Zide, and A. C. Gossard, *Appl. Phys. Lett.* **88**, 242107 (3pp) (2006).
5. G. Nolas, J. Sharp, and H. Goldsmid, *Thermoelectrics: Basic Principles and New Materials Developments*, Springer, 2001, chap. Historical Development.
6. H. Goldsmid, *Introduction to Thermoelectricity*, Springer, 2010, chap. Review of Thermoelectric Materials.
7. L. Weber, and E. Gmelin, *Appl. Phys. A* **53**, 136–140 (1991).
8. N. Neophytou, M. Wagner, H. Kosina, and S. Selberherr, *J. Electron. Mater.* **39**, 1902–1908 (2010).

9. J. Tang, H.-T. Wang, D. Lee, M. Fardy, Z. Huo, T. Russell, and P. Yang, *Nano Letters* **10**, 4279–4283 (2010).
10. W. Evans, L. Hu, and P. Keblinski, *Appl.Phys.Lett.* **96**, 203112 (2010).
11. J.-W. Jiang, J. Lan, J.-S. Wang, and B. Li, *J.Appl.Phys.* **107**, 054314 (2010).
12. J. Hu, S. Schiffli, A. Vallabhaneni, X. Ruan, and Y. Chen, *Appl.Phys.Lett.* **97**, 133107 (2010).
13. J. Hu, X. Ruan, and Y. Chen, *Nano Letters* **9**, 2730–2735 (2009).
14. H. Sevincli, and G. Cuniberti, *Phys.Rev.B* **81**, 113401 (2010).
15. X. Ni, G. Liang, J.-S. Wang, and B. Li, *Appl.Phys.Lett.* **95**, 192114 (2009).
16. K. Novoselov, A. Geim, S. Morozov, D. Jiang, Y. Zhang, S. Dubonos, I. Grigorieva, and A. Firsov, *Science* **5696**, 666–669 (2004).
17. A. Neto, F. Guinea, N. Peres, K. Novoselov, and A. Geim, *Rev.Mod.Phys.* **81**, 109–162 (2009).
18. Y. Huang, C. Chang, and M. Lin, *Nanotechnology* **18**, 495401 (2007).
19. T. Pedersen, C. Flindt, J. Pedersen, A.-P. Jauho, N. Mortensen, and K. Pedersen, *Phys.Rev.B* **77**, 245431 (2008).
20. D. Prezzi, D. Varsano, A. Ruini, A. Marini, and E. Molinari, *Phys.Rev.B* **77**, 041404(R) (2008).
21. A. Balandin, S. Ghosh, W. Bao, I. Calizo, D. Teweldebrhan, F. Miao, and C. Lau, *Nano Letters* **8**, 902–907 (2008).
22. D. Nika, S. Ghosh, E. Pokatilov, and A. Balandin, *Appl.Phys.Lett.* **94**, 203103 (2009).
23. K. Saito, J. Nakamura, and A. Natori, *Phys.Rev.B* **76**, 115409 (2007).
24. K. Kim, Y. Zhao, H. Jang, S. Lee, J. Kim, K. Kim, J.-H. Ahn, P. Kim, J.-Y. Choi, and B. Hong, *Nature* **457**, 706–710 (2009).
25. J.-H. Chen, C. Jang, S. Xiao, M. Ishigami, and M. Fuhrer, *Nature Nanotechnology* **3**, 206–209 (2008).
26. D. Dragoman, and M. Dragoman, *Appl.Phys.Lett.* **91**, 203116 (2007).
27. D. Nika, E. Pokatilov, A. Askerov, and A. Balandin, *Phys.Rev.B* **79**, 155413 (2009).
28. J. Hone, M. Whitney, C. Piskoti, and A. Zettl, *Phys.Rev.B* **59**, R2514–R2516 (1999).
29. J. Bai, X. Zhong, S. Jiang, Y. Huang, and X. Duan, *Nature Nanotechnology* **5**, 190–194 (2010).
30. J. Furst, J. Pedersen, C. Flindt, N. Mortensen, M. Brandbyge, T. Pedersen, and A.-P. Jauho, *New J. Phys.* **11**, 095020 (2009).
31. T. Pedersen, C. Flindt, J. Pedersen, N. Mortensen, A.-P. Jauho, and K. Pedersen, *Phys.Rev.Lett.* **100**, 136804 (2008).
32. D. Gunlycke, and C. White, *Phys.Rev.B* **77**, 115116 (2008).
33. R. Saito, G. Dresselhaus, and M. Dresselhaus, , *Physical Properties of Carbon Nanotubes*, Imperial College Press, 1998, chap. Phonon Modes of Carbon Nanotubes.
34. R. Kim, S. Datta, and M. Lundstrom, *J. Appl. Phys.* **105**, 034506 (6pp) (2009).
35. Y. Ouyang, and J. Guo, *Appl. Phys. Lett.* **94**, 263107 (3pp) (2009).